Available online at www.sciencedirect.com
SCIENCE DIRECT®
Journal of Sound and Vibration 289 (2006) 612–631
JOURNAL OF SOUND AND VIBRATION
www.elsevier.com/locate/jsvi

Aeroelastic flutter of a disk rotating in an unbounded acoustic medium

Anirban Jana, Arvind Raman*

School of Mechanical Engineering, Purdue University, West Lafayette, IN 47907-2088, USA

Received 26 September 2003; received in revised form 7 February 2005; accepted 15 February 2005
Available online 5 July 2005

Abstract

The linear aeroelastic stability of an unbaffled flexible disk rotating in an unbounded fluid is investigated by modeling the disk–fluid system as a rotating Kirchhoff plate coupled to the irrotational motions of a compressible inviscid fluid. A perturbed eigenvalue formulation is used to compute systematically the coupled system eigenvalues. Both a semi-analytical and a numerical method are employed to solve the fluid boundary value problem. The semi-analytical approach involves a perturbation series solution of the dual integral equations arising from the fluid boundary value problem. The numerical approach is a boundary element method based on the Hadamard finite part. Unlike previous works, it is found that a disk with zero material damping destabilizes immediately beyond its lowest critical speed. Upon the inclusion of small disk material damping, the flutter speeds become supercritical and increase with decreasing fluid density. The competing effects of radiation damping into the surrounding fluid and disk material damping control the onset of flutter at supercritical speed. The results are expected to be relevant for the design of rotating disk systems in data storage, turbomachinery and manufacturing applications.

1. Introduction

Aeroelastic flutter poses serious challenges in the design of high-speed disks rotating in air. Some practical examples are idling circular saws and CD and DVD drives. In the case of idling saws, aeroelastic flutter will generate noise and may also hamper the precise engagement of the

*Corresponding author. Tel.: +1 765 494 5733; fax: +1 765 494 0539.
E-mail address: raman@ecn.purdue.edu (A. Raman).

0022-460X/$ - see front matter © 2005 Elsevier Ltd. All rights reserved.
doi:10.1016/j.jsv.2005.02.042

saw with the workpiece. In high-speed CD and DVD drives, aeroelastic flutter can cause read–write errors and increased noise emissions. This directly limits operation speeds and data transfer rates in such devices. Aeroelastic flutter may also constrain the future design of microscale turbomachines where the rotor resembles a thin disk and the operating speeds are extremely high (millions of rev/min).

A systematic study of aeroelastic flutter of rotating disks began with the experiments of Stakhiev [1], which demonstrated that disks flutter with large amplitude beyond certain rotation speeds, and that these vibrations vanish in vacuum. Later Bouchard and Talke [2] showed a significant reduction in the disk vibration amplitudes at subcritical speeds when the surrounding air is replaced by helium. These early observations indicate that vibrations of a spinning disk may be profoundly affected by the surrounding fluid.

More detailed experimental and theoretical investigations of aerodynamically induced instabilities in rotating disks have been attempted recently. One body of research concerns the flutter of rotating disks supported on very thin air films [3–6]. This problem is relevant in the design of floppy and zip disk systems. Because of the low Reynolds number of the fluid film, these analyses use the incompressible Reynolds' equation of classical hydrodynamic lubrication theory to couple the film pressure to the disk vibration. However, such models are inapplicable for a disk rotating in an unbounded fluid medium or in a fluid-filled enclosure where the gap between the disk and enclosure wall is large.

D'Angelo and Mote [7] published extensive experimental results on the flutter of a thin steel disk rotating in open air as well as in an enclosed nitrogen atmosphere at controlled densities. They measured the flutter speeds, and growths of vibration amplitude with increasing rotation speed before and after flutter. Their measurements show an initial small increase in vibration amplitude as the disk passes critical speed, followed by rapid growth in the amplitude after the flutter instability. The fluttering traveling waves were visualized using Moiŕe photography, providing direct evidence that the flutter is due to the instability of a single reflected traveling wave (RTW). For the enclosed disk, they demonstrated that the measured flutter speeds increase with decreasing fluid density.

Some ad hoc rotating damping models have been proposed to predict aeroelastic flutter in disks rotating in an unbounded fluid or a large fluid-filled enclosure. Yasuda et al. [8] presented an ad hoc model to predict the flutter speed of a disk rotating in an unbounded fluid. They proposed that the aerodynamic load on the disk be expressed as a combination of "damping" and "lift" terms. This representation of the non-conservative aerodynamic load models a distributed rotating damping. However, they did not provide a physical basis for the above representation of the aerodynamic load. Hansen et al. [9] suggested an experimental method for predicting flutter of a disk rotating in a fluid, based on the rotating damping model. They extracted, from measurements of the frequency response of the spinning disk, the ratio of the"lift" to "damping" coefficients. Their method exploited the differential damping of forward and backward traveling waves (FTW and BTW) reported by Yasuda et al. and also observed much earlier by Campbell [10] and Tobias and Arnold [11]. However, while a systematic experimental parameter extraction procedure was provided, their use of generalized rotating damping models is somewhat ad hoc. No relationship was predicted between the rotating damping pressure and known disk and fluid properties and geometry. Kim et al. [12] extended the above experimental technique to predict the flutter speed of an enclosed rotating disk (a hard disk drive).

A few detailed theoretical models have also been proposed to explain aeroelastic flutter in disks rotating in an unbounded fluid or a large fluid-filled enclosure. Renshaw et al. [13] attempted the theoretical modeling of aeroelastic flutter of materially *undamped* disks using compressible, potential flow aerodynamics and identified three dimensionless parameters characterizing the stability of the fluid–disk system. Both enclosed and unenclosed disks were considered. However, their theoretical predictions only qualitatively matched experiments. Their predicted theoretical flutter speeds exceeded experimental values by several orders of magnitude. Kim and Renshaw [14] presented an alternative theoretical model for predicting the aeroelastic flutter of a rotating disk in an unbounded fluid. They considered the oscillations of a rotating compressible fluid coupled to a flexible, materially *undamped* co-rotating disk. They provided a simple model based on the assumption that the compressibility effects are confined to a thin boundary layer near the disk periphery. Their predicted flutter speeds exceed experimental values by less than an order of magnitude. Kang and Raman [15] have recently published a detailed study on different aeroelastic instability mechanisms in a disk rotating in an *enclosed* compressible fluid. However, the acoustic–structure interactions considered in Ref. [15] are very different from those arising in an unbounded fluid.

This paper re-examines the aeroelastic flutter of an unbaffled flexible disk rotating in an unbounded fluid. The main contributions of this paper are (a) to compute systematically the eigenvalues of the coupled disk–fluid system by employing a perturbed eigenvalue formulation combined with semi-analytical/numerical solution of the fluid boundary value problem (BVP), (b) to demonstrate that a materially undamped disk destabilizes immediately beyond its lowest critical speed, (c) to investigate the effect of the disk material damping on the aeroelastic stability of the rotating disk, and (d) to highlight the crucial competing effects of radiation damping into the surrounding fluid and disk material damping on the onset of the aeroelastic instability.

Section 2 models the disk–fluid system as a rotating Kirchhoff plate coupled to the irrotational motions of a compressible inviscid fluid, following Renshaw et al. [13]. Section 3 outlines the perturbed eigenvalue formulation, which enables a systematic computation of the coupled system eigenvalues. To solve the fluid governing equations and compute the eigenvalue perturbations, both a semi-analytical and a numerical approach are employed. The semi-analytical approach consists of the derivation of a pair of dual integral equations from the fluid BVP, followed by a perturbation solution of these dual integral equations. Section 4 presents this approach and its predictions. The numerical approach is a boundary element technique to solve directly the fluid BVP. Section 5 outlines this approach and its predictions. Section 6 briefly compares the theoretical predictions of this work with previously published results and provides some suggestions for improved flutter predictions. Finally, the conclusions are listed in Section 7.

2. Field equations for the disk–fluid system

An annular disk of uniform thickness h, clamped at inner radius a and free at outer radius b, rotates about its axis in the counter-clockwise direction at a constant angular speed Ω, as shown in Fig. 1. The disk is thin, homogeneous, isotropic and linearly elastic, with mass density ρ_d, Young's modulus E and Poisson's ratio ν. It is surrounded by an inviscid compressible fluid of ambient density ρ_f and acoustic velocity c_0 ($\Omega b < c_0$). The fluid is unbounded and there are no acoustically

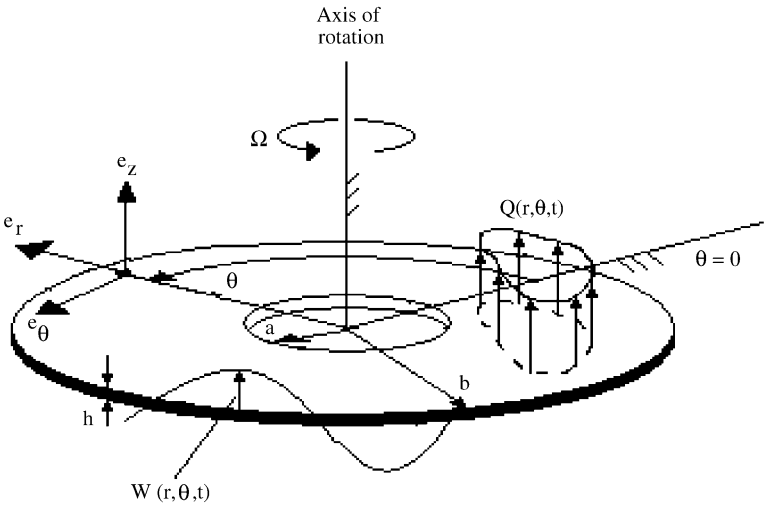

Fig. 1. The aerodynamically loaded rotating disk and its associated ground-fixed basis.

reflective surfaces in the vicinity of the disk. $(\mathbf{e}_r, \mathbf{e}_\theta, \mathbf{e}_z)$ form the cylindrical basis for a ground-fixed reference frame, with its origin fixed at the intersection of the mid-plane of the disk and its axis, and $\mathbf{e}_z$ oriented along this axis. Our model for this disk–fluid system is based on the aeroelastic model formulated by Renshaw et al. [13].

An Eulerian description of the transverse displacement $w(r, \theta, t)$ of the mid-plane of the disk, which is modeled as a Kirchhoff plate with rotation-dependent membrane stresses, results in the following equation [9,16]:

$$\rho_d h(w_{,tt} + 2\Omega w_{,t\theta} + \Omega^2 w_{,\theta\theta}) + C_d(w_{,t} + \Omega w_{,\theta}) + D\nabla^4 w = Q(r, \theta, t) + \frac{h}{r}\left(r\sigma_{rr} w_{,r}\right)_{,r} + \frac{h}{r^2}\left(\sigma_{\theta\theta} w_{,\theta}\right)_{,\theta}. \tag{1}$$

Here ∇^4 is the biharmonic operator, C_d is the velocity-proportional disk material damping coefficient, $D = Eh^3/(12(1 - \nu^2))$ is the bending stiffness of the disk, $Q(r, \theta, t)$ is the distributed aerodynamic load on the disk and σ_{rr} and $\sigma_{\theta\theta}$ are the rotation induced radial and hoop membrane stresses. The expressions for σ_{rr} and $\sigma_{\theta\theta}$ are derived from classical plane-stress linear elasticity (see for example Ref. [17]).

The fluid motions are assumed to be irrotational, so that the fluid velocity $\mathbf{v}(r, \theta, z, t) = \nabla\phi$, where $\phi(r, \theta, z, t)$ is the fluid velocity potential. Assuming infinitesimal fluid motions, the dynamics of the fluid are modeled using linear acoustics. $\phi(r, \theta, z, t)$ is then governed by the free space wave equation

$$\nabla^2\phi = \frac{1}{c_0^2}\phi_{,tt}, \tag{2}$$

and the linearized fluid pressure is given by

$$p = -\rho_f \phi_{,t}. \tag{3}$$

The aerodynamic load on the disk, $Q(r,\theta,t)$ equals the fluid pressure differential across its top and bottom surfaces. Since the disk is thin,

$$Q = p(z=0^-) - p(z=0^+) = \rho_f(\phi_{,t}(z=0^+) - \phi_{,t}(z=0^-)). \tag{4}$$

ϕ can be written as the sum of components that are symmetric and antisymmetric with respect to the plane $z=0$:

$$\phi = \phi_s + \phi_a, \quad \phi_s(z) = \phi_s(-z), \quad \phi_a(z) = -\phi_a(-z).$$

Because the fluid pressure depends on the difference in $\phi_{,t}$ across the disk thickness, ϕ_s decouples from the equation of motion of the disk. In studying disk vibrations, therefore, it is sufficient to set $\phi_s = 0$ and $\phi = \phi_a$ [13]. Thus although disk vibrations may produce a non-zero ϕ_s in the fluid field, ϕ_s does not in turn effect the vibrations. Hence Eq. (4) for the aerodynamic load becomes

$$Q = 2\rho_f \phi_{,t}(z=0^+). \tag{5}$$

Introduction of the following non-dimensional quantities

$$r' = \frac{r}{b}, \quad z' = \frac{z}{b}, \quad a' = \frac{a}{b}, \quad t' = \frac{t}{b^2}\sqrt{\frac{D}{\rho_d h}}, \quad \Omega' = \frac{\mathrm{d}\theta}{\mathrm{d}t'}, \quad w' = \frac{bw}{h^2}, \quad \Lambda = \frac{b\rho_f}{h\rho_d},$$
$$C_d' = \frac{C_d b^2}{\sqrt{D\rho_d h}}, \quad \phi' = \frac{\phi b^2}{h^2}\sqrt{\frac{\rho_d h}{D}}, \quad c = \frac{c_0}{\sqrt{D/(\rho_d h b^2)}}, \quad p' = \frac{pb^5}{Dh^2}, \tag{6}$$

and combination of Eqs. (1) and (5) lead to the non-dimensional governing equation for transverse disk vibrations is obtained:

$$w_{,tt} + 2\Omega w_{,t\theta} + \Omega^2 w_{,\theta\theta} + C_d(w_{,t} + \Omega w_{,\theta}) + L_\Omega^{r\theta}(w) = 2\Lambda\phi_{,t}(z=0^+), \tag{7}$$

where the primes have been dropped. Here $L_\Omega^{r\theta}(w)$ is the linear stiffness operator for the in vacuo rotating disk, and includes the bending and membrane stiffness operators. For the form of $L_\Omega^{r\theta}(w)$, see for example Ref. [6] or Ref. [13]. Similarly, non-dimensionalization of the wave equation (2) and dropping of primes lead to

$$\nabla^2\phi = \frac{1}{c^2}\phi_{,tt}. \tag{8}$$

Boundary and far-field conditions must be appended to the field Eqs. (7) and (8). The disk is clamped at $r=a$ and free at $r=1$ (see Ref. [13] for mathematical forms of these boundary conditions). Further, the fluid normal velocity matches the disk velocity on the disk surface. Assuming that $w(r,\theta,t) = 0$ for $0<r<a$,

$$\phi_{,z} = w_{,t} \quad \text{for } 0<r<1,\ z=0. \tag{9}$$

Because the disk is unbaffled, the fluid velocity on $z=0$ off the disk surface is non-zero. However, provided no shock waves exist, ϕ is at least continuous across $z=0$ for $r>1$. In conjunction with our assumption that $\phi = \phi_a$, this requires

$$\phi = 0 \quad \text{for } r>1,\ z=0. \tag{10}$$

The far-field condition requires that fluid velocities remain finite, that is

$$\phi_{,r},\ (1/r)\phi_{,\theta},\ \phi_{,z} \text{ finite as } r^2+z^2\to\infty. \tag{11}$$

Note that six non-dimensional parameters characterize the problem. These are the clamping ratio, a, the Poisson's ratio, ν, the non-dimensional rotation speed, Ω, the non-dimensional disk material damping, C_d, the ratio of fluid-to-disk densities, Λ, and the ratio of acoustic speed in fluid to a bending wave speed in disk, c.

3. The eigenvalue perturbation method

The eigenvalue problem corresponding to the free vibrations of the system (7) and (8) is derived by assuming the following separable forms in time and space [13]:

$$w(r,\theta,t)=W(r,\theta)\mathrm{e}^{\lambda t},\quad \phi(r,\theta,z,t)=\Phi(r,\theta,z)\mathrm{e}^{\lambda t}. \tag{12}$$

Substitution of the above solution forms into Eq. (7) yields the differential eigenvalue problem for transverse disk vibration coupled to the surrounding fluid:

$$\lambda^2 W+2\Omega\lambda W_{,\theta}+\Omega^2 W_{,\theta\theta}+C_d(\lambda W+\Omega W_{,\theta})+L_\Omega^{r\theta}(W)=2\Lambda\lambda\Phi(z=0). \tag{13}$$

Because C_d and Λ are usually small in practical applications, the eigenvalue problem (13) can be viewed as slightly perturbed from the eigenvalue problem for the undamped, in vacuo rotating disk. The eigensolutions for the present problem can then be computed by using eigenvalue perturbation theory [18] as follows. Let (λ_k, W_k) be an eigenvalue–eigenfunction pair for the present problem and let the corresponding Φ be denoted by Φ_k. λ_k, W_k and Φ_k can each be expanded in a perturbation series with Λ as the perturbation parameter:

$$\begin{aligned}\lambda_k&=\lambda_k^{(0)}+\Lambda\lambda_k^{(1)}+\mathcal{O}(\Lambda^2),\\ W_k&=W_k^{(0)}+\Lambda W_k^{(1)}+\mathcal{O}(\Lambda^2),\\ \Phi_k&=\Phi_k^{(0)}+\Lambda\Phi_k^{(1)}+\mathcal{O}(\Lambda^2),\end{aligned} \tag{14}$$

where

$$(\lambda_k^{(0)}, W_k^{(0)})=(\pm\mathrm{i}\omega_{mnb}, W_{mn}(r)\mathrm{e}^{\pm\mathrm{i}n\theta})\quad\text{or}\quad(\pm\mathrm{i}\omega_{mnf}, W_{mn}(r)\mathrm{e}^{\mp\mathrm{i}n\theta}) \tag{15}$$

are the well-known BTW and FTW eigensolutions for an undamped, in vacuo rotating disk. Beyond critical speed, a BTW is referred to as a reflected traveling wave (RTW). Here m and n denote the numbers of nodal circles and nodal diameters, respectively. Substituting the series expansions (14) in Eq. (13), assuming $C_d\sim\mathcal{O}(\Lambda)$, and equating terms of $\mathcal{O}(\Lambda)$ from both sides leads to

$$\begin{aligned}&\lambda_k^{(0)^2}W_k^{(1)}+2\lambda_k^{(1)}\lambda_k^{(0)}W_k^{(0)}+2\Omega\left(\lambda_k^{(1)}W_{k,\theta}^{(0)}+\lambda_k^{(0)}W_{k,\theta}^{(1)}\right)+\Omega^2W_{k,\theta\theta}^{(1)}\\&\quad+\frac{C_d}{\Lambda}\left(\lambda_k^{(0)}W_k^{(0)}+\Omega W_{k,\theta}^{(0)}\right)+L_\Omega^{r\theta}(W_k^{(1)})=2\lambda_k^{(0)}\Phi_k^{(0)}(z=0).\end{aligned} \tag{16}$$

In order to obtain an expression for $\lambda_k^{(1)}$ from Eq. (16), the following observations are first recorded:

(1) The in vacuo rotating disk eigenfunctions $W_k^{(0)}$ (expressions (15)) form a basis for the expansion of $W_k^{(1)}$.
(2) Both the disk displacement and the slope need to be 2π-periodic.
(3) Because the clamped–free disk boundary conditions are independent of the perturbation parameter Λ, any $W_k^{(j)}$ is a comparison function. Self-adjointness of the operator $L_\Omega^{r\theta}(\bullet)$ implies, in particular, that $\langle L_\Omega^{r\theta}(W_k^{(1)}), W_l^{(0)}\rangle = \langle W_k^{(1)}, L_\Omega^{r\theta}(W_l^{(0)})\rangle$, where $\langle \bullet, \bullet\rangle$ is the usual complex inner product [19].
(4) Experiments [7,13] demonstrate that aeroelastic flutter in rotating disks is due to the instability of a RTW. Hence only BTW/RTW eigenvalues are of interest in studying the stability of the disk–fluid system. Thus henceforth, the index k represents a specific (m,n) BTW/RTW. In particular, $\lambda_k^{(0)} = \mathrm{i}\omega_{mnb}$. That no FTW eigenvalue can cross into the right half-plane resulting in flutter will also be clear in Section 4.3.

Now, taking the inner product of Eq. (16) with $W_k^{(0)}$, and simplifying the resulting expressions based on the above observations leads to

$$\lambda_k^{(1)} = \frac{\omega_{mnb} d_{kk}}{\omega_{mnb} + n\Omega} - \frac{C_d}{2\Lambda}, \tag{17}$$

where $d_{kk} = \langle \Phi_k^{(0)}(z=0), W_k^{(0)}\rangle$ represents the effect of the aerodynamic load on $\lambda_k^{(1)}$. Eq. (17) provides a convenient way to compute the $\mathcal{O}(\Lambda)$ corrections, $\lambda_k^{(1)}$, to the in vacuo (m,n) BTW/RTW eigenvalues of the disk–fluid system. $\lambda_k^{(1)}$ will in general be complex, its imaginary part signifying added fluid inertia and its real part consisting of competing contributions from radiation damping and disk material damping. Because $\lambda_k^{(0)}$ is purely imaginary, the kth BTW/RTW flutters whenever $\mathrm{Re}(\lambda_k^{(1)})$ changes sign from negative to positive.

The quantity d_{kk}, and hence $\lambda_k^{(1)}$, depends on $\Phi_k^{(0)}(z=0)$. Substitution of the separable forms (12) and perturbation expansions (14) into the wave equation (8) and the boundary and far field conditions (9)–(11) and retention of $\mathcal{O}(\Lambda)$ terms lead to

$$\nabla^2 \Phi_k^{(0)} = -\frac{\omega_{mnb}^2}{c^2} \Phi_k^{(0)} \tag{18}$$

and

$$\Phi_{k,z}^{(0)}(z=0) = \mathrm{i}\omega_{mnb} W_k^{(0)}, \quad 0<r<1, \tag{19a}$$

$$\Phi_k^{(0)}(z=0) = 0, \quad r>1, \tag{19b}$$

$$\Phi_{k,r}^{(0)},\ \frac{1}{r}\Phi_{k,\theta}^{(0)},\ \Phi_{k,z}^{(0)} \text{ finite as } r^2+z^2 \to \infty.$$

Therefore $\Phi_k^{(0)}$ is the fluid velocity potential generated by the disk vibrating in its kth in vacuo traveling wave mode. In the following sections, a semi-analytical and a numerical technique are developed to solve the fluid BVP (18) and (19) and obtain $\Phi_k^{(0)}(z=0)$ for each in vacuo mode and over a range of disk rotation speeds.

Table 1
Properties of the steel disk (from D'Angelo and Mote), in air

Property	Disk–fluid system
Outer diameter (mm)	356
Inner diameter (mm)	106.7
Thickness (mm)	0.775
Young's modulus (GPa)	207
Poisson's ratio	0.3
Density of disk (kg/m^3)	7700
Density of air (kg/m^3)	1.2
Speed of sound (m/s)	340

Note that both the semi-analytical and numerical methods involve the in vacuo spinning disk frequencies and radial eigenfunctions. In what follows, these are computed by Galerkin's method using the in vacuo stationary disk mode shapes as comparison functions. It was found that using the first four stationary disk modes with n nodal diameters in the eigenfunction expansion for the (m, n) in vacuo spinning disk mode ensures convergence of the in vacuo spinning disk frequencies upto at least four significant figures. The properties of the disk–fluid system chosen for all calculations in this paper are shown in Table 1.

4. Semi-analytical solution of the fluid boundary value problem

4.1. Dual integral equations

The mixed boundary value problem (18) and (19) for the fluid is first reduced to a pair of dual integral equations [13]. Assuming circumferential periodicity of the velocity potential,

$$\Phi_k^{(0)}(r,\theta,z) = \widehat{\Phi}_k(r,z)\mathrm{e}^{\mathrm{i}n\theta}, \tag{20}$$

substitution of Eq. (20) into Eq. (18), setting $\kappa = \omega_{mnb}/c$ and further simplification lead to

$$\widehat{\Phi}_{k,rr} + \frac{1}{r}\widehat{\Phi}_{k,r} + \widehat{\Phi}_{k,zz} - \left(\frac{n^2}{r^2} - \kappa^2\right)\widehat{\Phi}_k = 0. \tag{21}$$

The boundary and far-field conditions for $\widehat{\Phi}_k(r,z)$ can be derived from Eqs. (19).

Taking the Hankel transform of order n of Eq. (21) leads to [20]

$$\bar{\Phi}_{k,zz} - (\xi^2 - \kappa^2)\bar{\Phi}_k = 0, \tag{22}$$

where $\bar{\Phi}_k(\xi,z) = \int_0^\infty \widehat{\Phi}_k(r,z)J_n(\xi r)r\,\mathrm{d}r$ is the Hankel transform of order n of $\widehat{\Phi}_k(r,z)$ and $J_n(x)$ is the Bessel function of the first kind of order n. The general solution of Eq. (22) is given by

$$\bar{\Phi}_k(\xi,z) = A(\xi)\mathrm{e}^{\alpha(\xi)z} + B(\xi)\mathrm{e}^{-\alpha(\xi)z}, \tag{23}$$

where $\alpha(\xi) = \mathrm{i}\sqrt{\kappa^2 - \xi^2}$ if $\xi < \kappa$ and $\alpha(\xi) = \sqrt{\xi^2 - \kappa^2}$ if $\xi > \kappa$. Taking the inverse Hankel transform of Eq. (23) leads to

$$\widehat{\Phi}_k(r,z) = \int_0^{\kappa} \left(A(\xi)\mathrm{e}^{\mathrm{i}z\sqrt{\kappa^2-\xi^2}} + B(\xi)\mathrm{e}^{-\mathrm{i}z\sqrt{\kappa^2-\xi^2}} \right) J_n(\xi r)\xi \,\mathrm{d}\xi + \int_{\kappa}^{\infty} \left(A(\xi)\mathrm{e}^{z\sqrt{\xi^2-\kappa^2}} + B(\xi)\mathrm{e}^{-z\sqrt{\xi^2-\kappa^2}} \right) J_n(\xi r)\xi \,\mathrm{d}\xi. \tag{24}$$

To ensure that $\widehat{\Phi}_k(r,z)\mathrm{e}^{\mathrm{i}(n\theta+\omega_{mnb}t)}$ appears to a stationary observer located on the positive z-axis in the far field as a wave traveling in the positive z-direction, $A(\xi) = 0$ in the first integral. Because the far-field conditions require that gradients of $\widehat{\Phi}_k$ remain finite far away from the disk, $A(\xi) = 0$ in the second integral also. Substitution of the above form for $\widehat{\Phi}_k(r,z)$ with $B(\xi) = \mathrm{i}\omega_{mnb}b(\xi)/\xi$ and $A(\xi) = 0$ into the boundary conditions (19a,b) results in the following pair of dual integral equations:

$$\int_0^{\infty} \alpha(\xi)b(\xi)J_n(\xi r)\,\mathrm{d}\xi = -W_{mn}(r) \quad \text{for } 0<r<1,$$
$$\int_0^{\infty} b(\xi)J_n(\xi r)\,\mathrm{d}\xi = 0 \quad \text{for } r>1. \tag{25}$$

4.2. Solution of the dual integral equations in the vicinity of critical speed

The dual integral equations (25) are solved for $b(\xi)$ for each BTW/RTW near its critical speed by resorting to a series solution. Recall that the critical speed for the (m,n) BTW is the rotation speed at which ω_{mnb} vanishes. In a small neighborhood of this critical speed, the wavenumber $\kappa = \omega_{mnb}/c \ll 1$ can be used as a perturbation parameter in the series solution. This solution procedure was originally developed by King [21] in his work on the acoustic field generated by an oscillating, unbaffled, rigid piston. Our approach is an extension of King's method to enable the analysis of flexible disks. Renshaw et al. [13] also used a similar approach to solve the current problem, however details of the solution procedure were omitted. Moreover, our predictions are very different from Renshaw et al. [13].

Let

$$b(\xi) = b_0(\xi) + \widetilde{b}_1(\xi), \tag{26}$$

where $b_0(\xi)$ satisfies

$$\int_0^{\infty} \xi b_0(\xi)J_n(\xi r)\,\mathrm{d}\xi = -W_{mn}(r) \quad \text{for } 0<r<1,$$
$$\int_0^{\infty} b_0(\xi)J_n(\xi r)\,\mathrm{d}\xi = 0 \quad \text{for } r>1. \tag{27}$$

Eqs. (27) are a pair of Titchmarsh's equations with a known closed-form solution [22,23]:

$$b_0(\xi) = -\sqrt{\frac{2\xi}{\pi}} \int_0^1 t^{3/2} J_{n+1/2}(\xi t) \int_0^1 \frac{\tau^{n+1}}{\sqrt{1-\tau^2}} W_{mn}(t\tau)\,\mathrm{d}\tau\,\mathrm{d}t. \tag{28}$$

Substitution of Eqs. (26) and (27) into Eq. (25) leads to a pair of dual integral equations in $\widetilde{b}_1(\xi)$:

$$\int_0^\infty \alpha(\xi)\widetilde{b}_1(\xi)J_n(\xi r)\,\mathrm{d}\xi = \int_0^\kappa \xi b_0(\xi)J_n(\xi r)\,\mathrm{d}\xi - \int_0^\kappa \alpha(\xi)b_0(\xi)J_n(\xi r)\,\mathrm{d}\xi + \int_\kappa^\infty (\xi-\alpha(\xi))b_0(\xi)J_n(\xi r)\,\mathrm{d}\xi \quad \text{for } 0<r<1, \tag{29a}$$

$$\int_0^\infty \widetilde{b}_1(\xi)J_n(\xi r)\,\mathrm{d}\xi = 0 \quad \text{for } r>1. \tag{29b}$$

Expansion of each of the three integrals on the right-hand side of Eq. (29a) as a series in κ and evaluation of their sum leads to

$$\begin{aligned}\int_0^\infty \alpha(\xi)\widetilde{b}_1(\xi)J_n(\xi r)\,\mathrm{d}\xi &= -\kappa^2 F_1(r) \quad \text{for } 0<r<1,\\ \int_0^\infty \widetilde{b}_1(\xi)J_n(\xi r)\,\mathrm{d}\xi &= 0 \quad \text{for } r>1.\end{aligned} \tag{30}$$

where the derivation of an expression for $F_1(r)$ has been outlined in the Appendix. Next, set

$$\widetilde{b}_1(\xi) = b_1(\xi) + \widetilde{b}_2(\xi), \tag{31}$$

where $b_1(\xi)$ satisfies

$$\begin{aligned}\int_0^\infty \xi b_1(\xi)J_n(\xi r)\,\mathrm{d}\xi &= -\kappa^2 F_1(r) \quad \text{for } 0<r<1,\\ \int_0^\infty b_1(\xi)J_n(\xi r)\,\mathrm{d}\xi &= 0 \quad \text{for } r>1.\end{aligned} \tag{32}$$

Eqs. (32) are another pair of Titchmarsh's equations. Hence $b_1(\xi)$ has the same closed-form expression as $b_0(\xi)$ (Eq. (28)), with $W_{mn}(t\tau)$ replaced by $\kappa^2 F_1(t\tau)$. It is also observed that $\mathrm{Re}(b_1(\xi))\sim\mathcal{O}(\kappa^2)$ and $\mathrm{Im}(b_1(\xi))\sim\mathcal{O}(\kappa^{2n+3})$. Substitution of Eqs. (31) and (32) into Eq. (30) leads to a pair of dual integral equations for $\widetilde{b}_2(\xi)$. These steps can be repeated to yield expressions for higher-order terms of the series solution.

Summation of all orders to obtain the series solution $b(\xi) = b_0(\xi) + b_1(\xi) + \cdots$, combination of Eqs. (20) and (24) to obtain an expression for $\Phi_k^{(0)}(z=0)$ and computation of the inner product of $\Phi_k^{(0)}(z=0)$ with $W_{mn}^{(0)}$ determines d_{kk}. Substitution of d_{kk} into Eq. (17), use of Sonine and Schafheitlin's formula [24] to evaluate the improper integral over ξ and simplification leads finally to the following expressions for the real and imaginary parts of the $\mathcal{O}(\Lambda)$ eigenvalue correction, $\lambda_k^{(1)}$, to the kth in vacuo BTW/RTW frequency in a small neighborhood of its critical speed:

$$\mathrm{Re}(\lambda_k^{(1)}) = -\frac{C_d}{2\Lambda} - \frac{\sqrt{\pi}c^2\kappa^{2n+5}g_{00}\ n!}{2^{2n+1}(\Gamma(n+\frac{3}{2}))^2\Gamma(n+\frac{5}{2})(\omega_{mnb}+n\Omega)}\int_a^1 r^{n+1}\sqrt{1-r^2}\,W_{mn}(r)\,\mathrm{d}r + \mathcal{O}(\kappa^{2n+7}), \tag{33a}$$

$$\mathrm{Im}(\lambda_k^{(1)}) = -\frac{4\omega_{mnb}}{\omega_{mnb}+n\Omega}\int_a^1 r^{n+1}W_{mnb}(r)\int_r^1 \frac{1}{t^n\sqrt{1-r^2/t^2}}\int_{a/t}^1 \frac{\tau^{n+1}W_{mn}(t\tau)}{\sqrt{1-\tau^2}}\,\mathrm{d}\tau\,\mathrm{d}t\,\mathrm{d}r + \mathcal{O}(\kappa^2). \tag{33b}$$

Here m and n are the nodal circle and diameter numbers of the kth mode, $\Gamma(x)$ is the Gamma function and an expression for g_{00} is provided in Appendix A.

4.3. Flutter predictions using the semi-analytical solution

For materially undamped disks ($C_d = 0$), the flutter speed Ω_f of the kth BTW/RTW mode coincides exactly with its critical speed Ω_c. Note that $\kappa = \omega_{mnb}/c$ vanishes at the critical speed $\Omega = \Omega_c$ of that specific BTW/RTW mode [11]. ω_{mnb} and κ are positive at subcritical and negative at supercritical speeds. Since expression (33a) for $\mathrm{Re}(\lambda_k^{(1)})$ contains an odd power of κ, it is evident analytically that $\mathrm{Re}(\lambda_k^{(1)})$ changes sign from negative to positive at the critical speed of the kth BTW. Consequently, the disk destabilizes immediately beyond its lowest critical speed. Note that κ never changes sign for a FTW. Thus a FTW cannot undergo aeroelastic flutter.

This result is in accordance with the theorems of Kelvin, Tait and Chetaev (KTC) on dissipation-induced destabilization of gyroscopically stabilized systems [25]. For rotating disks, the total stiffness operator $\Omega^2(\bullet)_{,\theta\theta} + L_\Omega^{r\theta}(\bullet)$ loses positive definiteness at the critical speed. In vacuum, the disk is immediately gyroscopically stabilized and no instability is observed at supercritical speeds. According to the KTC theorem, however, the presence of the slightest positive definite damping destabilizes a gyroscopically stabilized system. When the disk rotates in air, the radiation damping plays the role of a small positive definite damping, causing the disk to destabilize immediately beyond its lowest critical speed. In this sense, the onset of flutter instability in a materially undamped disk occurs at its lowest critical speed.

Another interesting observation is that at the onset of the above flutter instability, the pair of complex conjugate eigenvalues for the fluttering BTW crosses into the right half-plane through the origin and the rate of change of their real part with rotation speed also vanishes ($\lambda_k^{(1)} = 0$ and $\mathrm{dRe}(\lambda_k^{(1)})/\mathrm{d}\Omega = 0$ at $\Omega = \Omega_f = \Omega_c$). This introduces an additional complication to the classical double-zero eigenvalue instability in damped, axisymmetric, gyroscopic systems near critical speed [26]. Complicated post-flutter dynamics may arise in the vicinity of such a degenerate bifurcation.

The imaginary part of $\lambda_k^{(1)}$ is a correction to the in vacuo frequency of the kth mode and signifies an added fluid inertia effect. In comparison to the in vacuo case, the added fluid inertia effect lowers the BTW/RTW frequencies at subcritical speeds but raises the BTW/RTW frequencies at supercritical speeds. The percentage change in the frequency due to the added fluid inertia is very small, and is speed dependent. The critical speeds, however, remain unaffected by the fluid loading.

For a materially damped disk with $C_d \sim \mathcal{O}(\Lambda)$, $\mathrm{Re}(\lambda_k^{(1)})$ changes sign when its radiation damping component becomes sufficiently positive to overcome the negative material damping component. This typically occurs at $\kappa > 1$, where the above perturbation solution becomes invalid. A numerical solution of the fluid BVP is needed to predict flutter speeds in this case.

5. Numerical solution of the fluid BVP

5.1. The boundary element method (BEM)

For the numerical solution of the fluid BVP, a BEM based on the Hadamard finite part is employed in this paper. This method has been developed in detail in a paper by Beslin and Nicolas [27]. A very brief outline is provided here.

The pressure at a point $\mathbf{M}$ exterior to a vibrating surface $\mathbf{S}$ due to the acoustic field generated by $\mathbf{S}$ is given by [28]

$$p(\mathbf{M}) = \int_{\mathbf{S}} (p(Q)\nabla G - G\nabla p(Q)) \cdot \mathbf{n}_s \, \mathrm{d}S(Q), \quad Q \in S, \tag{34}$$

where $G = \mathrm{e}^{-\mathrm{i}\kappa R(\mathbf{M},\mathbf{Q})}/(4\pi R(\mathbf{M},\mathbf{Q}))$ is the free space Green's function, $R(\mathbf{M},\mathbf{Q})$ is the distance between the field point $\mathbf{M}$ and the source point $\mathbf{Q}$ and $\mathbf{n}_s$ is the outward normal to $\mathbf{S}$ at $\mathbf{Q}$. For a thin disk, the contribution to the surface integral from the lateral cylindrical surface is negligible. Equal and opposite contributions from the upper and lower flat disk surfaces nullify the second term in the surface integral. The remaining term simplifies to

$$p(\mathbf{M}) = \int_{\mathbf{S}^+} \bar{p}(\mathbf{Q}) \frac{\partial G}{\partial z_{\mathbf{Q}}} \, \mathrm{d}S(\mathbf{Q}), \tag{35}$$

where $\mathbf{S}^+$ denotes the top surface of the disk and $\bar{p}(\mathbf{Q}) = p(\mathbf{Q}^+) - p(\mathbf{Q}^-)$ is the pressure jump across the vibrating disk.

The above integral relation is singular for $\mathbf{M} = \mathbf{Q}^* \in \mathbf{S}^+$. One way to circumvent this singularity is by considering the Hadamard finite part, where the limit of Eq. (35) as $\mathbf{M} \to \mathbf{Q}^*$, along the normal to $\mathbf{S}^+$ at $\mathbf{Q}^*$, is taken. The linearized Euler equation [28] relates the pressure and fluid normal velocity at $\mathbf{Q}^*$, and the latter equals the disk transverse velocity at $\mathbf{Q}^*$ due to the velocity matching boundary condition (19a). The integral over $\mathbf{S}^+$ in these relations is approximated as a finite sum by dividing $\mathbf{S}^+$ into N surface elements and assuming that the pressure over each element $\mathbf{S}_m$ is constant and equal to its value at the element centroid. This yields a system of N algebraic equations,

$$\mathbf{K}\bar{\mathbf{P}} = \mathrm{i}\omega_{mnb}\mathbf{W}, \tag{36}$$

where $\bar{\mathbf{P}}$ and $\mathbf{W}$ are $N \times 1$ vectors of the pressure jump and disk displacement amplitudes, respectively at the N collocation points (element centroids). $\mathbf{K}$ is a fully populated, complex, non-symmetric matrix. Its off-diagonal elements are given by

$$K_{nm} = \frac{1}{4\pi\Lambda c} \sum_{j=1}^{N_m} \kappa^2 s_{mj} \frac{1 + \mathrm{i}\kappa R(Q_{mj}, Q_n)}{(\mathrm{i}\kappa R(Q_{mj}, Q_n))^3} \mathrm{e}^{-\mathrm{i}\kappa R(Q_{mj}, Q_n)}, \quad m, n = 1, 2, \ldots, N, \; m \neq n, \tag{37}$$

where $\mathbf{S}_m$ is further subdivided into N_m regions $\mathbf{S}_{mj}$ having areas s_{mj} (see Fig. 2). The diagonal elements of $\mathbf{K}$ are evaluated in the sense of the Hadamard finite part by a semi-analytical integration [27], and are expressed as

$$K_{nn} = \frac{1}{4\pi\Lambda c} \sum_{j=1}^{N_n} \alpha_{nj} \left(1 + \frac{\mathrm{e}^{-\mathrm{i}\kappa a_{nj}}}{\mathrm{i}\kappa a_{nj}}\right), \quad n = 1, 2, \ldots, N, \tag{38}$$

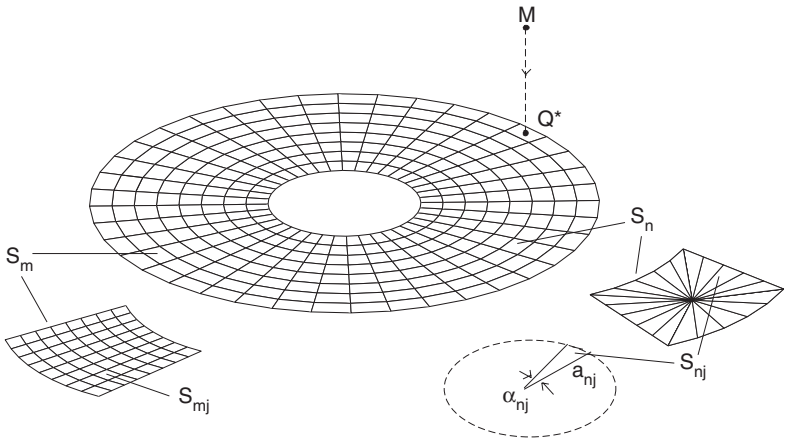

Fig. 2. Schematic of the boundary element method.

where $\mathbf{S}_n$ is further subdivided into N_n regions $\mathbf{S}_{nj}$. For a description of α_{nj} and a_{nj}, see Fig. 2 and Ref. [27].

In solving the fluid BVP (18) and (19) for a given kth in vacuo BTW mode, $\mathbf{W}$ in Eq. (36) is known, and is used to compute the unknown $\bar{\mathbf{P}}$. Noting that

$$\Phi_k^{(0)}(Q^+) = -\bar{P}(Q)/(2\mathrm{i}\omega_{mnb}\Lambda), \tag{39}$$

the inner product d_{kk} can then be computed for this mode through a simple numerical integration:

$$d_{kk} = \langle \Phi_k^{(0)}(z=0), W_k^{(0)} \rangle \approx -\frac{1}{2\mathrm{i}\omega_{mnb}\Lambda} \sum_{n=1}^{N} \bar{P}(Q_n) W_k^{(0)}(Q_n) s_n. \tag{40}$$

Using these computed d_{kk} values in Eq. (17), the $\mathcal{O}(\Lambda)$ eigenvalue corrections $\lambda_k^{(1)}$ are easily determined. Note that unlike the semi-analytical method, the above numerical method does not require the small wavenumber assumption. This method can thus be used for flutter prediction in disks with small but non-zero material damping.

5.2. Flutter predictions using the numerical method

Flutter predictions using the BEM are performed for the steel disk in D'Angelo and Mote's experiment [7]. The disk rotates in air at room temperature and pressure. The properties of this disk–fluid system are given in Table 1. For the in vacuo undamped rotating disk, the Galerkin computations indicate that the lowest non-dimensional critical speed is $\Omega_c = 5.746$ (or 2099 rev/min) and is associated with the (0, 3) BTW mode. This computed critical speed is very close to the experimentally measured in vacuo critical speed of 2078 rev/min [7]. The mesh used for the BEM consists of 3000 surface elements, formed by a grid of 120 radial and 25 concentric circular lines. For the computation of the off-diagonal entries of $\mathbf{K}$, each surface element is subdivided into $N_m = 625$ regions. For the diagonal entries of $\mathbf{K}$, each surface element is subdivided into $N_n = 100$ regions. A convergence study was performed to investigate the effect of mesh density on the

eigenvalue correction predictions. This study showed that the above choice of mesh density limits the errors in the resulting $\lambda_k^{(1)}$ values to less than 1%.

For $C_d = 0$, the variations with non-dimensional rotation speed Ω of the real and imaginary parts of the $\mathcal{O}(\Lambda)$ corrections to several in vacuo BTW/RTW eigenvalues are shown in Fig. 3. The corresponding insets show magnified views of the same in the speed range from $\Omega = 0$ to $\Omega = 7$. It is seen that the (0,3) BTW/RTW destabilizes first at its (and the disk's lowest) critical speed, $\Omega_f = \Omega_c = \Omega_{c3} = 5.746$. The plots corroborate all the conclusions for materially undamped disks inferred from the semi-analytical approach, including the coincidence of flutter speed with critical speed, and the non-degeneracy of the bifurcation.

Next, the effect of disk material damping on the onset of flutter is investigated. First, $C_d \approx 2.817 \times 10^{-14}$ is artificially chosen to give $\Omega_f = \Omega_{f3} \approx 7.504$ at $\Lambda \approx 0.034$, which is the flutter speed of the disk found experimentally in D'Angelo and Mote [7]. Using this damping estimate, the variation of flutter speed in rev/min with the density ratio Λ is computed for several BTW/RTW modes (Fig. 4). The results show that the flutter speed is now supercritical at which the frequency of the fluttering RTW is non-zero, and the flutter instability is a classical Hopf bifurcation of the equilibrium. Moreover, unlike the materially undamped case, the lowest flutter speed and the corresponding fluttering mode are now dependent on the density ratio Λ. For $\Lambda > 0.00115$, the (0, 3) BTW/RTW destabilizes first. But for $0.0005 < \Lambda < 0.00115$, the (0, 4) BTW/RTW destabilizes first. This exchange in the initial fluttering mode has been reported in Ref. [7]. Also, the lowest flutter speed Ω_f increases with decreasing Λ in a manner similar to the experimental observations in Ref. [7] (see Fig. 4). To summarize, the numerical predictions are in good correspondence with known experimental results. However, $C_d = 2.817 \times 10^{-14}$ is an unrealistically small value for the material damping coefficient of a real disk.

A more realistic value of $C_d = 0.00521$ is estimated from the in vacuo experimental data in Hansen et al. [9]. Note that both Refs. [7,9] employed exactly the same disk in their experiments. The variation of Ω_f (in rev/min) with Λ is recomputed for several BTW/RTW modes (Fig. 5).

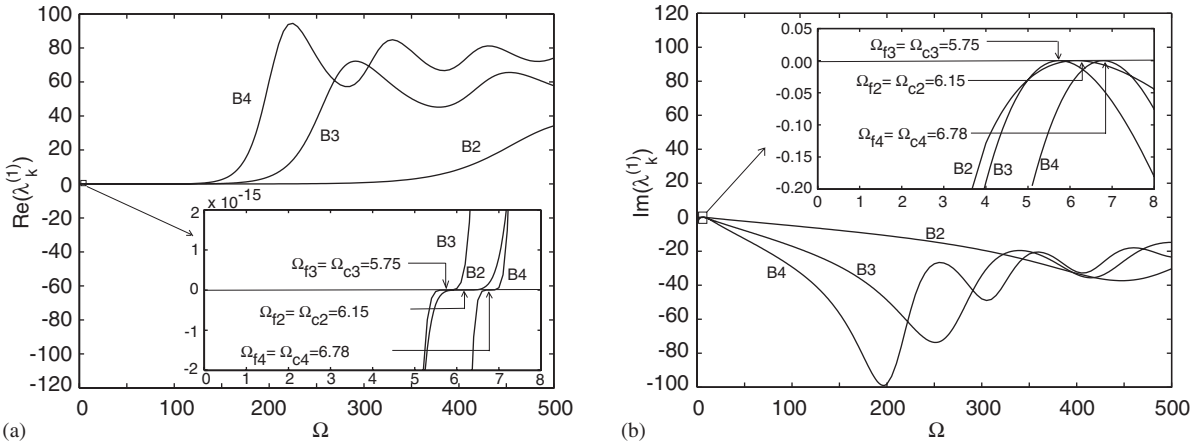

Fig. 3. The variation of the $\mathcal{O}(\Lambda)$ eigenvalue perturbations $\lambda_k^{(1)}$ with non-dimensional rotation speed Ω for the (0, 2), (0, 3) and (0, 4) BTWs/RTWs (labeled as B2, B3 and B4, respectively) of the steel disk of D'Angelo and Mote in air with $C_d = 0$: (a) real part—radiation damping (b) imaginary part—added fluid inertia.

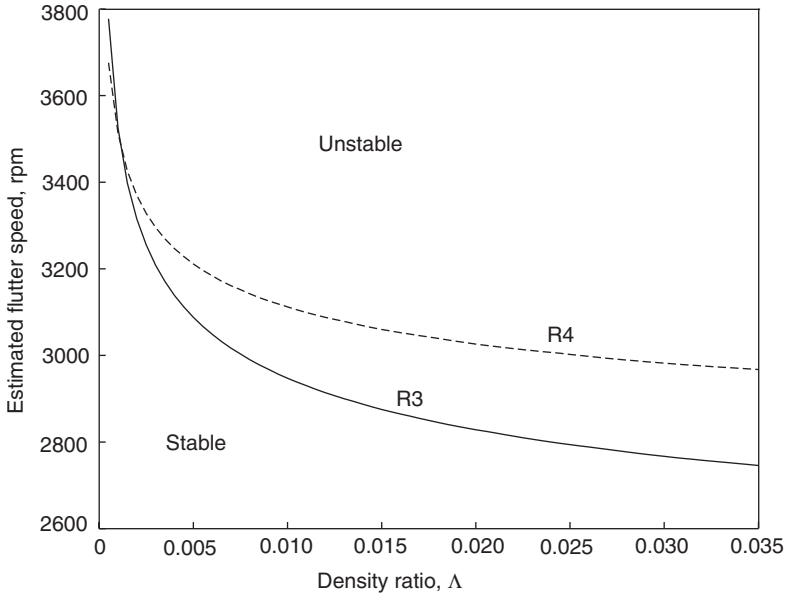

Fig. 4. Variation of flutter speed with the fluid-to-disk density ratio for the disk of D'Angelo and Mote, assuming $C_d = 2.817 \times 10^{-14}$. The labels R3 and R4 represent the $(0, 3)$ and $(0, 4)$ RTWs, respectively.

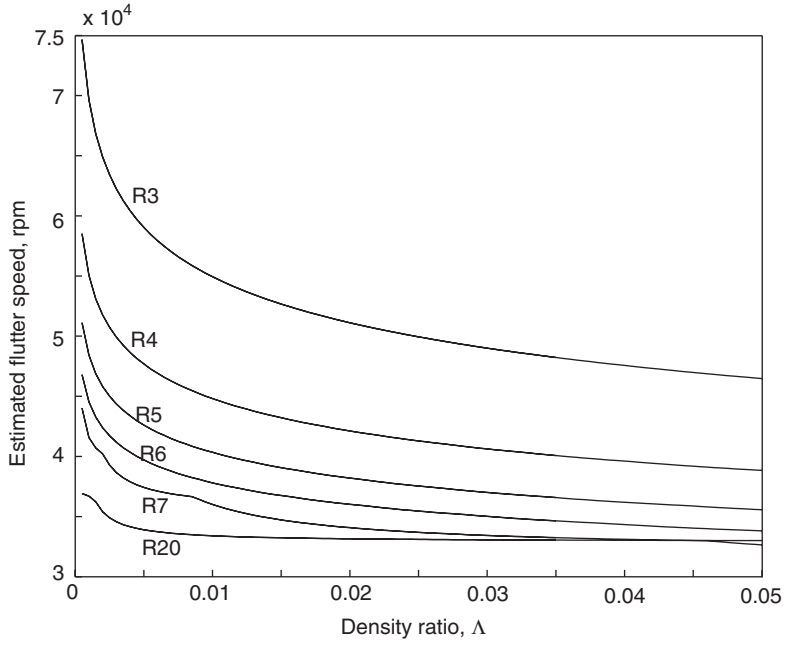

Fig. 5. Variation of flutter speed with the fluid-to-disk density ratio for the disk of D'Angelo and Mote, with $C_d = 0.00521$ (estimated from Hansen et al. [9]). The label R_n, $n = 3, 4, 5, 6, 7, 20$, represents the $(0, n)$ RTW.

Fig. 5 reveals important quantitative differences compared to the experimental observations in Ref. [7]. The computed flutter speeds are about an order of magnitude higher than experimental values reported in Ref. [7]. Additionally, the initial fluttering mode is no longer the (0, 3) RTW as observed experimentally. Instead, a very high nodal diameter RTW is likely to be the initial fluttering mode.

6. Discussions

6.1. Comparison with previous results

In this paper, essentially two potential flow aerodynamics based models for the disk–fluid system have been employed for studying its aeroelastic stability. The first model assumes zero disk material damping and predicts the onset of flutter exactly at the lowest disk critical speed. Previous experiments [7,13,14] have shown flutter speeds to be supercritical ($\Omega_f \approx 1.1\Omega_c$ to $1.5\Omega_c$ at room ambient density and even higher at lower ambient densities). Thus this model underpredicts the flutter speeds. For exactly the same model, Renshaw et al. [13] predicted flutter speeds that exceed experimental flutter speeds by several orders of magnitude. It is likely that this difference is due to their possible neglect of radiation damping (the second term in Eq. (33a)). The radiation damping term for a particular BTW/RTW, being $\mathcal{O}(\kappa^{2n+5})$, is extremely small near its critical speed, and may be overlooked in some solution schemes. The flutter mode predicted by this model is the RTW associated with the lowest critical speed. This flutter mode prediction matches with experiment at room ambient density [7]. Finally, unlike experiments [7,13,14], this model is incapable of capturing any dependence of the flutter speed and mode on the ambient density.

Upon refining the model to include small disk material damping, the predicted flutter speeds become supercritical and increase with decreasing fluid density as in experiments. With an artificial choice of the disk material damping, the experimentally observed dependence of the flutter mode on the ambient density can also be captured by the refined model. In this sense, the predictions of this refined model are qualitatively closer to experiments compared to the first model. However with a realistic value of the material damping coefficient C_d, the flutter speeds predicted by the refined model are higher than experimental flutter speeds and the predicted flutter mode is also incorrect.

The main reason for the somewhat anomalous predictions of the refined model is that the ground-fixed radiation damping for a BTW/RTW is extremely small in the vicinity of its critical speed. Moreover, away from the critical speed, the radiation damping effect increases with rotation speed much faster for higher nodal diameter RTWs compared to lower nodal diameter RTWs. This explains the theoretical prediction that higher nodal diameter modes flutter at lower rotation speeds than the lower nodal diameter modes.

Other reasons may also cause small discrepancies between the theoretical predictions and currently available experimental data. The experiments of Ref. [7] documenting the variation of flutter speed with ambient density were performed in an enclosure, albeit a large one. Even so, acoustic cavity modes may have affected the flutter phenomena. The current theory is for disks rotating in an unbounded fluid. Indeed, it will be difficult to experimentally vary the ambient

density in an unbounded setting. Also, the experimental disk material damping data in Ref. [9] exhibits large variations. More accurate experimental determination of material damping values will enhance the flutter predictions.

The flutter predictions of Kim and Renshaw [14] are arguably better than those of the refined model discussed above. Their predicted flutter speeds are less than an order of magnitude higher than experimental flutter speeds. Moreover, their predicted flutter mode is correct. However, their model is partially ad hoc and involves an arbitrary choice of a boundary layer weighting function to closely match theory with experiments. Note that our refined model with a realistic C_d value is devoid of ad hoc assumptions and entirely predictive.

6.2. Suggestions for improved flutter predictions

The current study clearly highlights the competing effects of the co-rotating disk material damping and the ground-fixed radiation damping that play a central role in the flutter mechanism. The ground-fixed radiation damping being extremely small in the vicinity of the critical speed, it is evident that any other unmodeled sources of ground fixed dissipation are crucial in causing the flutter instability in materially damped disks. Such additional damping mechanisms could arise due to incompressible perturbations of the Von Kármán swirling boundary layer controlled by convective and diffusive mechanisms. Inclusion of these additional damping effects is expected to provide closer agreement between theory and experiment even for realistic disk material damping values. However, a fluid model more sophisticated than potential flow aerodynamics is required to capture all these additional dissipative effects.

The flutter instability may also be influenced by compressible oscillations in the Von Kármán swirling boundary layer. The work of Kim and Renshaw [14] is an important step towards studying this effect. Future investigations of this effect may lead to further refinement in the prediction of the flutter instability.

7. Conclusions

The aeroelastic flutter of an unbaffled disk rotating in an unbounded fluid is analyzed by modeling the disk–fluid system as a centrifugally tensioned Kirchhoff plate coupled to irrotational flow of a compressible, inviscid, initially quiescent fluid. Infinitesimal disk deformations and linear acoustics for the fluid are assumed. Both disks with zero and small material damping are considered. A perturbed eigenvalue formulation is used to compute systematically the coupled system eigenvalues. A series solution of the dual integral equations, arising from the mixed BVP governing the fluid, predicts the onset of flutter in disks with zero material damping. For disks with small but non-zero material damping, a BEM is used instead.

The main conclusions of this study are:

(1) Compressible flow coupling leads to two distinct aerodynamic effects on disk vibration–radiation damping into the surrounding fluid and added fluid inertia effect.
(2) In the absence of disk material damping, the radiation damping destabilizes via a flutter instability the gyroscopically stabilized disk exactly at the critical speed. This onset of flutter

corresponds to a degenerate form of the double zero eigenvalue bifurcation of a damped gyroscopic system.

(3) With small disk material damping, the flutter speeds are supercritical and increase with decreasing fluid density. In this case, the instability is a classical Hopf bifurcation.

(4) For a very small value of disk material damping, the predicted flutter speeds and modes for different fluid-to-disk density ratios show good agreement with known experimental results. With a more realistic choice of the disk material damping, the predicted results remain qualitatively similar but differ quantatively from experiments.

(5) The added fluid inertia effect decreases slightly the frequencies of the BTWs, but increases slightly the frequencies of the RTWs. The critical speed is unaffected by the fluid loading.

To further improve the prediction of the flutter speeds and modes for materially damped disks, it is likely that additional dissipative effects need to be included in the model. Such dissipative effects could arise from fluid viscosity and compressibility in the Von Kármán swirling boundary layer, and is a subject of ongoing investigation.

Acknowledgements

The authors would like to thank the National Science Foundation (CAREER grant, Award No. 0134455-CMS) and the Purdue Research Foundation for financial support of this research.

Appendix A. Derivation of an expression for $F_1(r)$

An expression for the function $F_1(r)$ in Eq. (30) is derived here. The derivation involves expanding each of the three integrals on the right-hand side of Eq. (29a) as a series in κ. The first two integrals require the substitution $\xi = \kappa \sin\theta$. The third integral requires the substitution $\xi = \sqrt{\tilde{\xi}^2 + \kappa^2}$. These substitutions followed by expansion lead to

$$\begin{aligned}
\int_0^{\kappa} \xi b_0(\xi) J_n(\xi r)\,\mathrm{d}\xi = & -\frac{1}{\sqrt{\pi}}\left[\frac{\kappa^{2n+3} r^n g_{00}}{2^{2n+1}\Gamma(n+\frac{5}{2})\Gamma(n+1)} - \frac{\kappa^{2n+5} r^n}{2^{2n+3}\Gamma(n+\frac{7}{2})\Gamma(n+1)}\right. \\
& \left.\times\left(\left(\frac{n+\frac{3}{2}}{n+1}\right) r^2 g_{00} + g_{01}\right) + \cdots\right] \\
\int_0^{\kappa} \alpha(\xi) b_0(\xi) J_n(\xi r)\,\mathrm{d}\xi = & -\mathrm{i}\left[\frac{\kappa^{2n+3} r^n g_{00}}{2^{2n+2}\Gamma(n+\frac{3}{2})\Gamma(n+\frac{5}{2})} - \frac{\kappa^{2n+5} r^n}{2^{2n+4}\Gamma(n+\frac{3}{2})\Gamma(n+\frac{7}{2})}\right. \\
& \left.\times\left(r^2 g_{00} + \left(\frac{n+1}{n+\frac{3}{2}}\right) g_{01}\right) + \cdots\right] \\
\int_{\kappa}^{\infty} (\xi - \alpha(\xi)) b_0(\xi) J_n(\xi r)\,\mathrm{d}\xi = & -\frac{\kappa^2}{\sqrt{2\pi}} \int_0^1 t^{3/2} g_0(t) \int_0^{\infty} J_{n+\frac{1}{2}}(t\xi) J_n(r\xi) \xi^{-1/2}\,\mathrm{d}\xi\,\mathrm{d}t + \cdots, \qquad \text{(A.1)}
\end{aligned}$$

where

$$g_0(t) = \int_0^1 \frac{\tau^{n+1}}{\sqrt{1-\tau^2}} W_{mnb}(t\tau)\,\mathrm{d}\tau \tag{A.2}$$

and

$$g_{0j} = \int_0^1 t^{n+2+2j} g_0(t)\,\mathrm{d}t \quad \text{for } j = 0, 1, 2, \ldots\ . \tag{A.3}$$

Summing the three series given by Eqs. (A.1), it is seen that the sum is of $\mathcal{O}(\kappa^2)$. Setting it equal to $-\kappa^2 F_1(r)$, an expression for $F_1(r)$ is easily obtained.

References

[1] Y.M. Stakhiev, Vibrations in thin steel discs, *Russian Engineering Journal* 52 (1972) 14–17.
[2] G. Bouchard, F.E. Talke, Non-repeatable flutter of magnetic recording disks, *IEEE Transactions on Magnetics* 22 (5) (1986) 1019–1021.
[3] H. Hosaka, S.H. Crandall, Self-excited vibrations of a flexible disk rotating on an air film above a flat surface, *Acta Mechanica (Suppl)* 3 (1992) 115–127.
[4] F. Huang, C.D. Mote Jr., On the instability mechanisms of a disk rotating close to a rigid surface, *Journal of Applied Mechanics* 62 (1995) 764–771.
[5] A.A. Renshaw, Critical speed for floppy discs, *Journal of Applied Mechanics* 65 (1998) 116–120.
[6] G. Naganathan, S. Ramadhyani, A.K. Bajaj, Numerical simulations of flutter instability of a flexible disk rotating close to a rigid wall, *Journal of Vibration and Control* 9 (2002) 95–118.
[7] C. D'Angelo III, C.D. Mote Jr., Aerodynamically excited vibration and flutter of a thin disk rotating at supercritical speed, *Journal of Sound and Vibration* 168 (1) (1993) 15–30.
[8] K. Yasuda, T. Torii, T. Shimizu, Self-excited oscillations of a circular disk rotating in air, *JSME International Journal, Series III* 35 (3) (1992) 347–352.
[9] M.H. Hansen, A. Raman, C.D. Mote Jr., Estimation of nonconservative aerodynamic pressure leading to flutter of spinning disks, *Journal of Fluids and Structures* 15 (2001) 39–57.
[10] W. Campbell, The protection of steam-turbine disk wheels from axial vibration, *ASME Transactions* 46 (1924) 31–160.
[11] S.A. Tobias, R.N. Arnold, The influence of dynamical imperfection on the vibration of rotating disks, *Proceedings of the Institution of Mechanical Engineers, London* 171 (1957) 669–690
[12] B.C. Kim, A. Raman, C.D. Mote Jr., Prediction of aeroelastic flutter in a hard disk drive, *Journal of Sound and Vibration* 238 (2) (2000) 309–325.
[13] A.A. Renshaw, C. D'Angelo III, C.D. Mote Jr., Aerodynamically excited vibration of a rotating disc, *Journal of Sound and Vibration* 177 (5) (1994) 577–590.
[14] H.R. Kim, A.A. Renshaw, Aeroelastic flutter of circular disks: a simple predictive model, *Journal of Sound and Vibration* 256 (2) (2002) 227–248.
[15] N.C. Kang, A. Raman, Aeroelastic flutter mechanisms of a flexible disk rotating in an enclosed compressible fluid, *Journal of Applied Mechanics* 71 (1) (2004) 120–130.
[16] J.L. Nowinski, Nonlinear transverse vibrations of a spinning disk, *Journal of Applied Mechanics* 31 (1964) 72–78.
[17] I.S. Sokolnikoff, *Mathematical Theory of Elasticity*, McGraw-Hill, New York, 1956.
[18] R. Courant, D. Hilbert, *Methods of Mathematical Physics*, Vol. 1, Interscience Publishers, New York, 1953.
[19] I. Stakgold, *Green's Functions and Boundary Value Problems*, Wiley-Interscience, New York, 1998.
[20] I.N. Sneddon, *The Use of Integral Transforms*, McGraw-Hill, New York, 1972.
[21] L.V. King, On the acoustic radiation pressure on circular discs: inertia and diffraction corrections, *Proceedings of the Royal Society of London, Series A* 153 (1935) 1–16.

[22] I.N. Sneddon, *Mixed Boundary Value Problems in Potential Theory*, Wiley, New York, 1966.
[23] E.C. Titchmarsh, *Introduction to the Theory of Fourier Integrals*, The Clarenden Press, Oxford, 1948.
[24] G.N. Watson, *A Treatise on the Theory of Bessel Functions*, The University Press, Cambridge, 1952.
[25] D.R. Merkin, *Introduction to the Theory of Stability*, Springer, New York, 1997.
[26] S. Nagata, N.S. Namachchivaya, Bifurcations in gyroscopic systems with an application to rotating shafts, *Proceedings of the Royal Society of London, Series A* 454 (1970) (1998) 543–585.
[27] O. Beslin, J. Nicolas, Modal radiation from an unbaffled rotating disk, *Journal of the Acoustical Society of America* 100 (5) (1996) 3192–3202.
[28] A.D. Pierce, *Acoustics: An Introduction to its Physical Principles and Applications*, McGraw-Hill, New York, 1981.